SCIENCE CHINA
Physics, Mechanics & Astronomy

•Article•

July 2018 Vol. 61 No. 7: 076811
https://doi.org/10.1007/s11433-017-9169-7

Formation of a monolayer *h*-BN nanomesh on Rh (111) studied using *in-situ* STM

GuoCai Dong[1,3], Yi Zhang[2*], and Joost W. M. Frenken[4*]

[1]*Kamerlingh Onnes Laboratory, Leiden University, Leiden 2300 RA, The Netherlands;*
[2]*National Laboratory of Solid State Microstructure, School of Physics, Collaborative Innovation Center of Advanced Microstructures, Nanjing University, Nanjing 210093, China;*
[3]*Jiangnan Graphene Research Institute, Changzhou 213000, China;*
[4]*Advanced Research Center of Nanolithography, Amsterdam 1098 XG, The Netherlands*

Received November 30, 2017; accepted January 23, 2018; published online April 3, 2018

As a member of the 2D family of materials, *h*-BN is an intrinsic insulator and could be employed as a dielectric or insulating inter-layer in ultra-thin devices. Monolayer *h*-BN can be synthesized on Rh (111) surfaces using borazine as a precursor. Using *in-situ* variable-temperature scanning tunneling microscopy (STM), we directly observed the formation of *h*-BN in real-time. By analyzing the deposition under variable substrate temperatures and the filling rate of the *h*-BN overlayer vacant hollows during growth, we studied the growth kinetics of how the borazine molecules construct the *h*-BN overlayer grown on the Rh surface.

hexagonal boron nitride, STM, nanomesh

PACS number(s): 68.37.Ef, 68.65.-k, 81.16.-c

Citation: G. C. Dong, Y. Zhang, and J. W. M. Frenken, Formation of a monolayer *h*-BN nanomesh on Rh (111) studied using *in-situ* STM, Sci. China-Phys. Mech. Astron. **61**, 076811 (2018), https://doi.org/10.1007/s11433-017-9169-7

1 Introduction

In recent years, research into two-dimensional (2D) materials, including graphene, phosphorene, transition metal dichalcogenides, etc., has become a rapidly developing field [1,2]. Devices based on the vertically-stacked heterostructure of 2D materials show great advantages for many potential applications, such as high-performance and ultra-scaled transistors, flexible electronics, and highly effective photo voltaic devices [3-7]. As a member of the 2D family of materials, *h*-BN possesses a rather large band gap of ~6 eV, which gives it an insulating nature, therefore, it could be used in ultraviolet photoelectric devices [8-11]. Being free of dangling bonds and with a chemically inert surface, *h*-BN exhibits a dielectric breakdown strength of the same order of magnitude as conventional SiO_2 oxides [12,13], but induces much fewer or even free defects in the supported materials while acting as a substrate. For this reason, 2D layers on *h*-BN can exhibit ultra-higher electronic mobility than those on SiO_2 or other substrates [14-16]. Moreover, while consisting into a stacked heterostructure with other 2D materials, *h*-BN can further engineer the physical properties of the supporting layers, e.g., the *h*-BN substrate can induce a finite band gap in the supported graphene [17,18], and the light-matter interaction is enhanced in the graphene/*h*-BN van der Waals heterostructures [19]. Due to these advantages, *h*-BN is becoming one of most important candidates as ideal substrate, dielectric gating layer and insulating interlayer in the concepts of ultra-thin devices based on 2D materials, thus at-

*Corresponding authors (Yi Zhang, email: zhangyi@nju.edu.cn; Joost W. M. Frenken, email: j.frenken@arcnl.nl)

tracts more and more research interest [20-23].

Many researchers have reported that *h*-BN can be grown on transition metal surfaces by introducing borazine $(HBNH)_3$ or ammonia borane $(NH_3\text{-}BH_3)$ as a precursor [21,24-28]. Using a borazine precursor, a monolayer *h*-BN film can be synthesized on the Rh (111) surface at a growth temperature around 1000 K under ultra-high vacuum (UHV) environment [24]. Due to the lattice mismatch, the grown *h*-BN forms a corrugated structure, called a nanomesh [29]. In this study, using *in-situ* scanning tunneling microscopy (STM) with temperatures varied from room-temperature up to 1300 K, we directly observed the detailed growth procedure of a *h*-BN nanomesh formed on Rh (111), and investigated the kinetics of how borazine moves on the Rh (111) surface and finally forms the *h*-BN overlayer.

2 Methods

The experiments were carried out under UHV environment at base pressure of 1.5×10^{-11} mbar (1 mbar=100 Pa). A K-type thermocouple was spot-welded directly onto the Rh single crystal for monitoring the sample temperature. Clean Rh (111) surface was obtained by cycles of Ar^+ ion sputtering, followed by flash annealing to 1300 K, and post-exposure to 2×10^{-7}-3×10^{-7} mbar of O_2 for 1-2 h with a substrate temperature of 700-800 K. The last step proved necessary to remove the carbon contamination that segregated out of the bulk to the surface. Residual oxygen was removed from the Rh surface by flashing the sample to 1000 K. High-purity borazine, $(HBNH)_3$, was gratefully obtained from the group of Prof. Hermann Sachdev at the University of Saarland in Germany. This was introduced into the UHV chamber via a dosing nozzle, which stored the borazine at a reduced temperature, by means of a Peltier cooler, and allowed it to warm up for deposition purposes. The growth dynamics of the *h*-BN overlayer were characterized using *in-situ* variable-temperature STM with thermal compensation, which allowed fast scanning and imaging over a wide temperature range and during substantial temperature changes.

3 Results and discussion

To form a hexagonal boron nitride lattice, borazine molecule need to be dehydrogenized by breaking the B-H and N-H bonds, and the resulting $(\text{-B-N-})_3$ hexagon rings should be compacted into the *h*-BN lattice [24,28,30]. Thus, we exposed a Rh (111) substrate in borazine environment at different temperatures to investigate the role of substrate temperature. First, we kept the substrate at 627 K, then introduced borazine gas into the UHV chamber at a pressure of 3.2×10^{-9} mbar. Figure 1(a) shows an STM image of the Rh (111) surface after the deposition of borazine for 12 min. While the terraces on the Rh (111) surface exhibited a low density of nuclei, the step-edges were saturated with fractal-like islands without the characteristic corrugation of the *h*-BN nanomesh, indicating that they had not formed the *h*-BN structure yet. Then, we increased the sample temperature and simultaneously monitored the deposition using *in-situ* STM. Whereas at 762 K the islands still retained their fractal shapes, at 806 K they became compact and also occurred on the terraces (Figure 1(b)). These islands displayed a variety of orientations. The preferred orientation was one aligned with the *h*-BN lattice, and therefore the moiré pattern also aligned with the Rh (111) substrate.

On this *h*-BN seeded surface, with different orientations, further *h*-BN overlayer was formed by exposing the surface to borazine with pressures ranging from 1.2×10^{-9} to 1.2×10^{-8} mbar and at an increased substrate temperature of 865 K. Figure 1(c) and (d) show the same area before and after this extra deposition, respectively. They show that most of the additional *h*-BN closely followed the orientations of the "seed" islands (blue lines in Figure 1(d)). At every

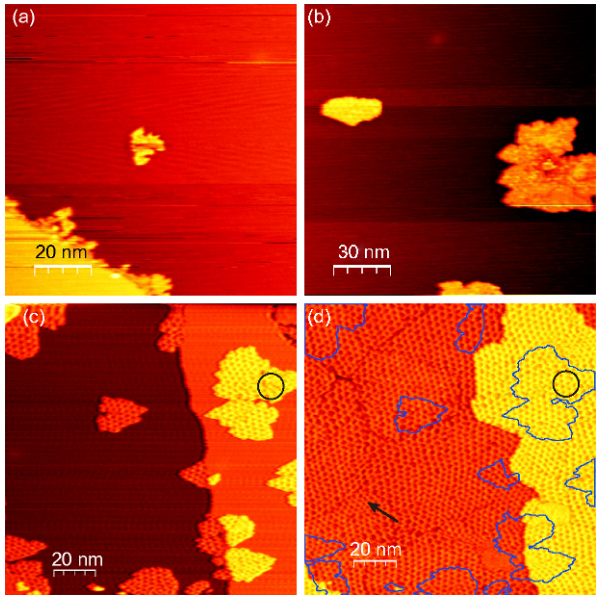

Figure 1 (Color online) (a) STM image of Rh (111) at 627 K, after exposure at that temperature to 3×10^{-9} mbar borazine for 12 min. The Rh steps are saturated by small fractal-like islands. (b) STM image after the substrate temperature increased to 806 K. The *h*-BN islands appear compact and the nanomesh superstructures can be observed within. The islands did not occur primarily at Rh substrate steps. (c) After a further temperature increase to 865 K, the islands become more compact. (d) The same area as in panel (c), after an additional borazine exposure at pressures ranging from 2×10^{-9} to 1.2×10^{-8} mbar for 78 min, while the temperature of the sample was kept at 865 K. The surface was fully covered by a *h*-BN overlay showing a variety of orientations. The blue lines indicate the contours of the initial islands in panel (c). Most of the growth followed the orientations of these initial islands. The black arrow indicates a new domain that formed during growth. Within the circles, the defects present in panel (c) have been removed. V_{bias} = 2.9, 2.8, −1.0, and −1.0 V for panels (a)-(d), respectively, I_t = 0.05 nA.

location where two domains met, a domain boundary line or a defect line was formed. However, some exceptions were observed. For example, the domain indicated by the black arrow in Figure 1(d) was newly formed at the connection between two differently-oriented domains, suggesting that in spite of the extra domain boundary length, a new domain can lower the total energy. In other words, the mismatch between these orientations was unfavorable. Further evidence was present in the initial islands. For example, the defect marked by a circle in Figure 1(c) is no longer present in Figure 1(d). However, when different domains encountered one another, the removal of defects occurred far less frequently than the formation of defect lines. As a result, the completed *h*-BN overlayer contained a significant density of defects. Thus, a higher substrate temperature (typically ~1000 K) is required to remove defects during growth.

In Figure 1, we see that the borazine molecule has not directly absorb onto the Rh (111) surface at the high temperature of ~627 K, but formed only a few nuclei on the terraces or step-edges. Between 762 and 806 K, the depositing borazine started to decompose. Therefore, to form a *h*-BN overlayer, a substrate temperature of 865 K or higher must be required during growth.

To further investigate how the borazine deposited on Rh surface and formed the *h*-BN overlayer, we observed the growth procedure of *h*-BN on Rh in real-time, with a substrate temperature of 978 K. Figure 2(a) and (b) show the *in-situ* STM images captured during and after a fully covered *h*-BN overlayer growth. It is obvious that a higher substrate temperature leads to fewer defects in the *h*-BN overlayer. The growth rate is expressed by the filling rate of the vacant hollows, namely the uncovered Rh surface, in Figure 2(c). Unlike traditional molecular beam epitaxial grown films, here we found that growth rate was not proportional to deposition time and below we suggest a simple model to explain the filling rate of the vacant hollows.

First, we assumed that the chemical potential and density of B and N atoms inside a vacant hollow are uniform, this holds true as long as the geometry of the hollow is not too complex to influence the diffusion of the surface species. Then, we assumed that only those borazine molecules that land on the bare metal surface can stick, decompose, and contribute to the formation of *h*-BN, due to the nature of the chemically inert surface of *h*-BN and the absence of a second layer on the *h*-BN overlayer. Thus, the time dependence of the total area of a vacant hollow can be calculated to satisfy

$$\frac{\mathrm{d}A}{\mathrm{d}t} = -\frac{A}{D}I\lambda = \frac{A}{D}\lambda\frac{P}{\sqrt{2\pi m k_{\mathrm{b}}T}} = -\alpha AP\lambda, \tag{1}$$

where, A is the area of the vacant hollow; P is the impinging borazine pressure; t is deposition time; λ represents the effective number of B and N atoms from borazine that contribute to the *h*-BN overlayer per impinging borazine molecule; D represents the areal density of B and N atoms in the *h*-BN overlayer. The impingement rate of borazine I can be expressed in terms of borazine gas pressure P, gas temperature T, and mass of a borazine molecule m, using standard kinetic gas theory. The part that remains unchanged during the deposition is combined in the constant α. Based on this differential equation, we expect exponential decay of the uncovered area as follows:

$$\ln\left(\frac{A}{A_0}\right) = \alpha P\lambda t. \tag{2}$$

Before testing this prediction experimentally, first we calibrated the relationship between the measured borazine pressure and the impinging flux of borazine molecules by exposing a fresh Rh surface to a low dose of 2.1×10^{-7} mbar of borazine at room temperature. We assumed that this temperature was low enough to inhibit the decomposition and desorption of the deposited molecules, and we assumed the resulting coverage to be low enough to avoid reflection of borazine molecules that impinged on other borazine molecules. From the coverage of adsorbed borazine molecules visible in the STM image, we obtained α=2.1 $\times10^{-5}$ mbar^{-1} s^{-1}, and an impingement rate on Rh (111) equivalent to 0.65 monolayers of *h*-BN per 10^{-6} mbar s of borazine exposure, where one monolayer is defined as a

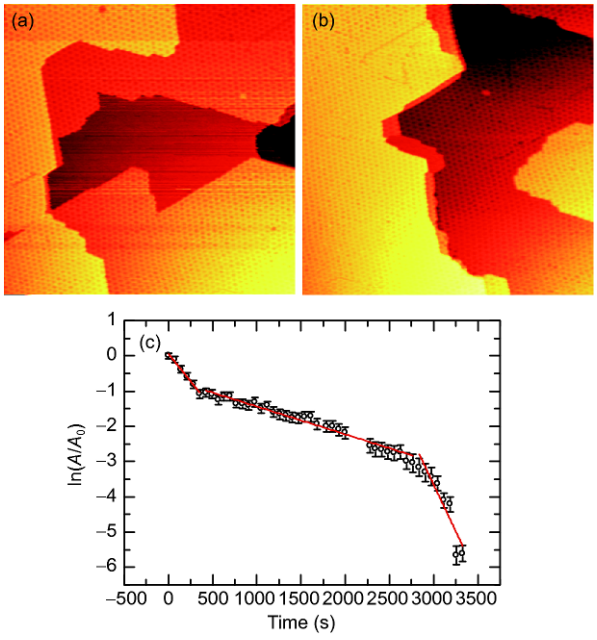

Figure 2 (Color online) STM images (170 nm×170 nm) at the beginning (a) and end (b) of the filling of a vacant hollow in the *h*-BN overlayer on Rh (111), with a substrate temperature of 978 K and borazine pressure of 3.2×10^{-9} mbar. (c) Time dependence of the area of the vacant hollow, relative to the area in panel (a). The slopes of the three linear fits to the initial, intermediate, and end stages of the process are -3.1×10^{-3}, -0.79×10^{-3}, and 5.1×10^{3} s^{-1} respectively, corresponding to λ-values of 4.6, 1.2, and 7.6 in eq. (2). As argued in the text, the values exceeding 3 indicate that a significant supply of B and N atoms originate from the lower Rh terrace, to which the vacant hollow is connected.

completely filled *h*-BN overlayer. Armed with this calibration, the λ-factor in eq. (1) can be accurately calculated.

Now we discuss the analysis of the filling rate of four vacant hollows shown in Figures 2-4. The data in the first two figures were extracted from the experiment at a substrate temperature of 978 K, while the data in Figure 4 was measured at a lower temperature of 865 K. Each of the figures shows the first and last images of the episodes that were analyzed, and the growth rate in each figure is a semi-logarithmic plot of the relative area of vacant hollows versus deposition time. The two plots in Figure 4 are for the two vacant hollows in the field of view. The prediction of eq. (2) should result in straight lines in these plots with a negative slope, from which the value of λ can be determined directly. Even though we can fit straight lines to the four semi-logarithmic area-versus-time plots, three of the curves deviate noticeably from linear behavior and become steeper toward the ends.

The λ-values obtained from the straight-line fits to the data in Figures 2(c) and 3(c) are higher than 3 (number of B-N pairs in one borazine molecule), namely 4.6 and 7.6 for the initial and end stages, respectively, in Figure 2(c), and 5.7 for the entire fit in Figure 3(c). We attribute these high values to the fact that these two vacant hollows were both connected to a part of the bare Rh surface that was either one atomic layer higher or lower, and that this area was not counted as part of the vacant hollows. We initially assumed that the diffusion of

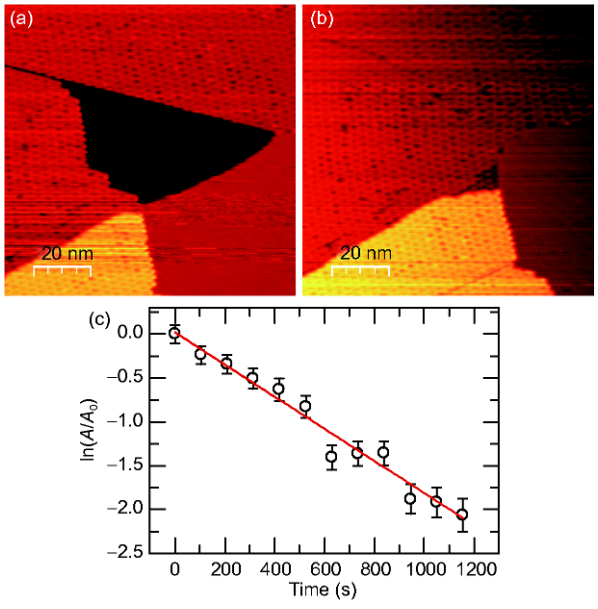

Figure 3 (Color online) STM images (100 nm×100 nm) at the beginning (a) and end (b) of the filling of a vacant hollow in the *h*-BN overlayer on Rh (111), with a substrate temperature of 978 K and borazine pressure of 1.5×10^{-9} mbar. (c) Time dependence of the area of the vacant hollow, relative to the area in panel (a). The slope of the linear fit of -1.8×10^{-3} s^{-1} corresponds to a λ-value of 5.7 in eq. (2). As argued in the text, this value, being higher than 3, indicates that a significant supply of B and N atoms originates from the higher Rh terrace on the right, to which the vacant hollow is connected.

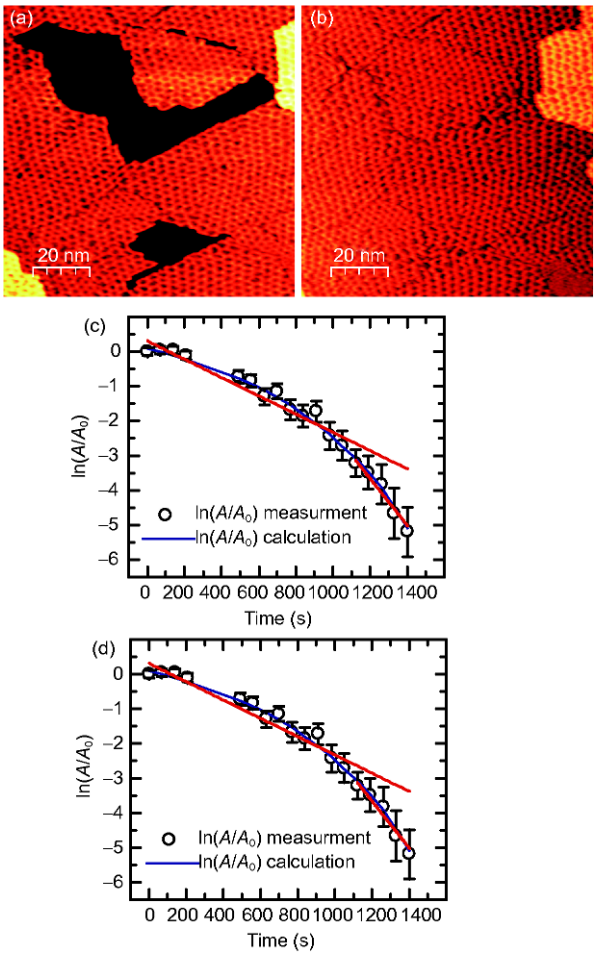

Figure 4 (Color online) STM images (100 nm×100 nm) at the beginning (a) and end (b) of the filling of two vacant hollows in the *h*-BN overlayer on Rh (111), with a substrate temperature of 865 K and borazine pressure of 1.0×10^{-8} mbar. In plots (c) and (d), the black circles are the time-dependent areas measured directly from the images of the upper and lower vacant islands, relative to their starting sizes in image (a). The linear fits for the full ranges in (c) and (d) have slopes of -2.25×10^{-3} and -2.64×10^{-3} s^{-1}, corresponding to λ-values of 1.0 and 1.2 in eq. (2). The slopes of the final sections of these two curves both correspond to λ=3, showing that all borazine impinging on the enclosed Rh is consumed in the final stages. The blue lines in (c) and (d) are the areas numerically calculated using eq. (4) with finite capture zone widths of w = 0.8 and 0.1 nm respectively.

B and N atoms across the steps between the Rh terraces would be strongly suppressed, but the high λ-values indicate that both vacant hollows were filled with a significant supply of B and N atoms from the adjacent Rh terraces.

The two vacant hollows in Figure 4 are fully enclosed by the *h*-BN overlayer, so there were no additional sources of B and N atoms available. If we fit straight lines to the area plot for these two hollows, we indeed find λ-values below 3, namely 1.2 for the upper hollow and 1.0 for the lower one. As already mentioned, both plot curves downward dramatically at the end stages. The slopes of the ends of both curves correspond to λ-values of 3.0, indicating that only during the end stages, when the vacant hollows are close to being

completely filled, do all the B and N atoms from the borazine molecules impinging on the remaining bare Rh 'enclaves' get fully incorporated into the *h*-BN overlayer. The fact that the two curves start with much more modest slopes shows that in larger vacant hollows, a significant fraction of the supplied borazine molecules (or B and N atoms) is desorbed from the Rh surface rather than incorporated into the *h*-BN overlayer. The corresponding finite residence time of the diffusing surface species (adsorbed borazine or B and N adatoms) implies that it can only reach the edge of the vacant hollow over a finite distance. In other words, there is a finite effective capture zone inside the contour of each vacant hollow. Borazine impinging within this zone is fully incorporated at the edges and contributes to the filling of the vacant hollow, whereas borazine that impinges on Rh but closer to the center, i.e., outside the capture zone, is destined to desorb. This scenario naturally explains the curvature of the measured area plots and suggests that we should modify the expected growth law according to:

$$\frac{\mathrm{d}A}{\mathrm{d}t} = -3\alpha wLP, \tag{3}$$

where, L is the length of the inner contour of the vacant hollow and w is the width of the capture zone, which is determined by the diffusion coefficient and residence time and should therefore depend on the substrate temperature. From this we obtain:

$$A(t) = A_0 - 3\alpha\omega P\int_{t_0}^{t} L(t)\mathrm{d}t. \tag{4}$$

We can check the validity of eq. (4) by integrating it numerically. The only free fitting parameter is the width w of the capture zone. The results for the upper and lower vacant hollows in Figure 4 are shown by blue lines in Figure 4(c) and (d) and the best-fit values of w are 0.8 and 1 nm, respectively. For both vacant hollows, this simple model provides an excellent description of the way they fill as a function of deposition time. The fact that the best-fit values of the capture zone widths are nearly identical provides extra confidence that eq. (3) meaningfully describes the growth process. The capture zone width is surprisingly small, which shows that at 865 K, most of the borazine impinging on the Rh surface already desorbs within a small number of diffusion steps.

The conclusion that the capture zone has a width in the order of 1 nm at 865 K seems to be in conflict with the fit in Figure 3(c), in which the value of λ corresponds to a large capture zone, larger than that of the enclosed Rh terrace and even including the part of the Rh surface on another adjacent terrace. A possible explanation could be that the higher substrate temperature at which the experiment shown in Figure 3 was performed makes decomposition of borazine to be possible at bare Rh, while at 865 K a *h*-BN edge or Rh step may be needed for the decomposition of borazine. Therefore, the B and N supply at 978 K would be much higher.

4 Conclusion

In conclusion, the role of the substrate in the desorption and decomposition of the borazine molecule was investigated. From the formation of a compact *h*-BN overlayer, we determined that the decomposition temperature of borazine on the Rh (111) surface is between 762 and 806 K. Borazine only decomposes on the Rh surface, while molecules landing on *h*-BN do not contribute to the growth of the overlayer. From the study of filling rates of *h*-BN vacant hollows during growth, we learned that with a substrate temperature of 865 K the effective capture zone for borazine molecules is 1 nm or less around the *h*-BN edge. At 978 K, the capture zone is much wider, and the B and N atoms can diffuse to higher or lower Rh terraces. This implies that at 865 K a *h*-BN edge or Rh terrace step may be needed for the decomposition of borazine, while at 978 K borazine decomposes on the Rh terraces.

This work was supported by the National Natural Science Foundation of China (Grant Nos. 51402026, 11774154, and 11790311), the Program for High-Level Entrepreneurial and Innovative Talents Introduction, Jiangsu Province, the Basic Research Program of Jiangsu Province (Grant No. BK20130236), and the National Key Research and Development Plan (Grant No. 2016YFE0125200).

1 M. Xu, T. Liang, M. Shi, and H. Chen, Chem. Rev. **113**, 3766 (2013).
2 S. Z. Butler, S. M. Hollen, L. Cao, Y. Cui, J. A. Gupta, H. R. Gutiérrez, T. F. Heinz, S. S. Hong, J. Huang, A. F. Ismach, E. Johnston-Halperin, M. Kuno, V. V. Plashnitsa, R. D. Robinson, R. S. Ruoff, S. Salahuddin, J. Shan, L. Shi, M. G. Spencer, M. Terrones, W. Windl, and J. E. Goldberger, ACS Nano **7**, 2898 (2013).
3 T. Niu, and A. Li, Prog. Surf. Sci. **90**, 21 (2015).
4 G. Fiori, F. Bonaccorso, G. Iannaccone, T. Palacios, D. Neumaier, A. Seabaugh, S. K. Banerjee, and L. Colombo, Nat. Nanotech. **9**, 768 (2014).
5 J. Yoon, W. Park, G. Y. Bae, Y. Kim, H. S. Jang, Y. Hyun, S. K. Lim, Y. H. Kahng, W. K. Hong, B. H. Lee, and H. C. Ko, Small **9**, 3295 (2013).
6 W. Han, R. K. Kawakami, M. Gmitra, and J. Fabian, Nat. Nanotech. **9**, 794 (2014), arXiv: 1503.02743.
7 Z. Liu, J. Gao, G. Zhang, Y. Cheng, and Y. W. Zhang, Nanotechnology **28**, 385704 (2017).
8 H. Zeng, C. Zhi, Z. Zhang, X. Wei, X. Wang, W. Guo, Y. Bando, and D. Golberg, Nano Lett. **10**, 5049 (2010).
9 Y. Lin, and J. W. Connell, Nanoscale **4**, 6908 (2012).
10 D. A. Laleyan, S. Zhao, S. Y. Woo, H. N. Tran, H. B. Le, T. Szkopek, H. Guo, G. A. Botton, and Z. Mi, Nano Lett. **17**, 3738 (2017).
11 R. Bourrellier, S. Meuret, A. Tararan, O. Stéphan, M. Kociak, L. H. G. Tizei, and A. Zobelli, Nano Lett. **16**, 4317 (2016).
12 Y. Hattori, T. Taniguchi, K. Watanabe, and K. Nagashio, ACS Nano **9**, 916 (2015).
13 Y. Hattori, T. Taniguchi, K. Watanabe, and K. Nagashio, Appl. Phys. Lett. **109**, 253111 (2016), arXiv: 1612.07557.
14 W. Gannett, W. Regan, K. Watanabe, T. Taniguchi, M. F. Crommie,

and A. Zettl, Appl. Phys. Lett. **98**, 242105 (2011), arXiv: 1105.4938.
15 J. Xie, Z. Y. Zhang, D. Z. Yang, M. S. Si, and D. S. Xue, arXiv: 161003185v2.
16 C. R. Dean, A. F. Young, I. Meric, C. Lee, L. Wang, S. Sorgenfrei, K. Watanabe, T. Taniguchi, P. Kim, K. L. Shepard, and J. Hone, Nat. Nanotech. **5**, 722 (2010), arXiv: 1005.4917.
17 N. Kharche, and S. K. Nayak, Nano Lett. **11**, 5274 (2011), arXiv: 1110.5702.
18 G. Giovannetti, P. A. Khomyakov, G. Brocks, P. J. Kelly, and J. van den Brink, Phys. Rev. B **76**, 073103 (2007), arXiv: 0704.1994.
19 W. Aggoune, C. Cocchi, D. Nabok, K. Rezouali, M. Akli Belkhir, and C. Draxl, J. Phys. Chem. Lett. **8**, 1464 (2017).
20 H. Wang, D. Lu, J. Kim, Z. Wang, S. T. Pi, and R. Q. Wu, Nanoscale **9**, 2974 (2017).
21 K. K. Kim, A. Hsu, X. Jia, S. M. Kim, Y. Shi, M. Dresselhaus, T. Palacios, and J. Kong, ACS Nano **6**, 8583 (2012).
22 M. P. Levendorf, C. J. Kim, L. Brown, P. Y. Huang, R. W. Havener, D. A. Muller, and J. Park, Nature **488**, 627 (2012).
23 C. Zhang, S. Zhao, C. Jin, A. L. Koh, Y. Zhou, W. Xu, Q. Li, Q. Xiong, H. Peng, and Z. Liu, Nat. Commun. **6**, 6519 (2015).
24 G. Dong, E. B. Fourré, F. C. Tabak, and J. W. M. Frenken, Phys. Rev. Lett. **104**, 096102 (2010).
25 R. Laskowski, and P. Blaha, Phys. Rev. B **81**, 075418 (2010).
26 F. Müller, S. Hüfner, H. Sachdev, R. Laskowski, P. Blaha, and K. Schwarz, Phys. Rev. B **82**, 113406 (2010).
27 L. Song, L. Ci, H. Lu, P. B. Sorokin, C. Jin, J. Ni, A. G. Kvashnin, D. G. Kvashnin, J. Lou, B. I. Yakobson, and P. M. Ajayan, Nano Lett. **10**, 3209 (2010).
28 G. Kim, A. R. Jang, H. Y. Jeong, Z. Lee, D. J. Kang, and H. S. Shin, Nano Lett. **13**, 1834 (2013).
29 M. Corso, W. Auwärter, M. Muntwiler, A. Tamai, T. Greber, and J. Osterwalder, Science **303**, 217 (2004).
30 A. P. Farkas, P. Török, F. Solymosi, J. Kiss, and Z. Kónya, Appl. Surf. Sci. **354**, 367 (2015).